Bull. Mater. Sci., Vol. 37, No. 1, February 2014, pp. 35–39. © Indian Academy of Sciences.

Analysis of Li-related defects in ZnO thin films influenced by annealing ambient

BING WANG* **and LIDAN TANG**
Department of Materials Science and Engineering, Liaoning University of Technology, Jinzhou 121001, China

MS received 28 July 2012; revised 21 September 2012

Abstract. **Li-doped ZnO thin films were grown on quartz substrates by radio frequency magnetron sputtering and *in situ* annealing under O_2 or Ar ambient. Li-related defects in ZnO films strongly depend on the annealing ambient. AFM and XRD indicated that ZnO films possessed a good crystallinity with *c*-axis orientation, uniform thickness and dense surface. Electrical and optical properties demonstrated that, an amount of Li_{Zn} defect had existed in ZnO annealed under O_2 ambient and an amount of $Li_{i(o)}$ defect had existed in ZnO annealed under Ar ambient. First-principle calculations were performed to calculate formation energies of Li-doped ZnO in order to explain the formation mechanism of Li-related defects in ZnO.**

Keywords. **ZnO; thin films; radio frequency magnetron sputtering.**

1. Introduction

Zinc oxide has attracted much attention as a promising material for short-wavelength optoelectronic devices, such as ultraviolet-light emitting diodes and laser diodes, because of its wide bandgap (3·37 eV) and large exciton binding energy (60 meV) (Osamu *et al* 2000; Look *et al* 2004). A key issue in exploring ZnO is the fabrication of *p*-type ZnO (Van de Walle 2000; Coppa *et al* 2003). Lithium doping in ZnO is usually carried out to control electrical properties. Li substituting for Zn theoretically possesses shallower acceptor levels (Zhang *et al* 2001; Shan *et al* 2007). Furthermore, Li element may be the best candidate in producing *p*-type ZnO due to almost no lattice relaxations around the impurity atom. But most of Li doped ZnO films were either *n*-type or semi-insulating (Joseph *et al* 2001; Look *et al* 2002) because Li incorporation occurs at interstitial sites as well as at substitution sites. Recently, there have been a number of efforts to characterize Li-related defect structure by studying defect-structure sensitive properties, such as impurity diffusion (Hu *et al* 2008) and electrical measurements (Look and Claflin 2004; Mohamed *et al* 2005). Here, we report the effects of annealing ambient on Li-related defects in ZnO films. Formation mechanism of Li-related defects in ZnO was studied by calculating formation energies of Li-related defects structure.

2. Experimental

Li-doped ZnO thin films are fabricated by radio frequency magnetron sputtering using a $Zn_{0·97}Li_{0·03}O$ ceramic target and *in-situ* annealing under O_2 or Ar ambient. Before sputtering, the chamber was evacuated to a base pressure of $\sim 10^{-4}$ Pa and then O_2 (sample A) and Ar (sample B) were introduced into it as the working gas with a pressure of ∼0·6 Pa. The rf power was 90 W and diameter of targets used was 50·5 mm. The substrate-to-target distance was about 18 cm. The deposition rate was 1·36 nm/min. During film deposition, the substrate temperature was maintained at 240 °C. Finally, the Li-doped ZnO films were annealed at 500 °C for 10 min.

The crystalline structure and morphology of obtained ZnO films were analysed by X-ray diffraction (XRD) (D/MAX-RB, CuKα) and scanning electron microscopy (SEM) (Zeiss, SUPRA-55), respectively. The transmission through the film was measured in the wavelength range from 300–800 nm by U-3400 Spectrometry. The electrical properties were obtained by the four-probe method using Hall-effect measurement system (HL5500PC).

Density functional calculations were performed to calculate the formation energies of Li-doped ZnO. PAW pseudopotential and PBE exchange correlation functional were employed in the calculations. *K*-point density is 3 nm and plane wave cutoff energy is 400 eV.

3. Results and discussion

3.1 *Structural properties*

Figure 1 (a) shows XRD patterns of Li-doped ZnO films annealed under O_2 (sample A) and Ar (sample B). In XRD patterns, one peak is observed at 34 ∼ 35° in both films, which corresponds to (002) diffraction face of ZnO. XRD analysis indicated that the films were crystallized in the wurtzite phase and presented a preferential orientation along *c*-axis. Furthermore, FHW of (002) diffraction peaks of

*Author for correspondence (lgclwb@yahoo.com.cn)

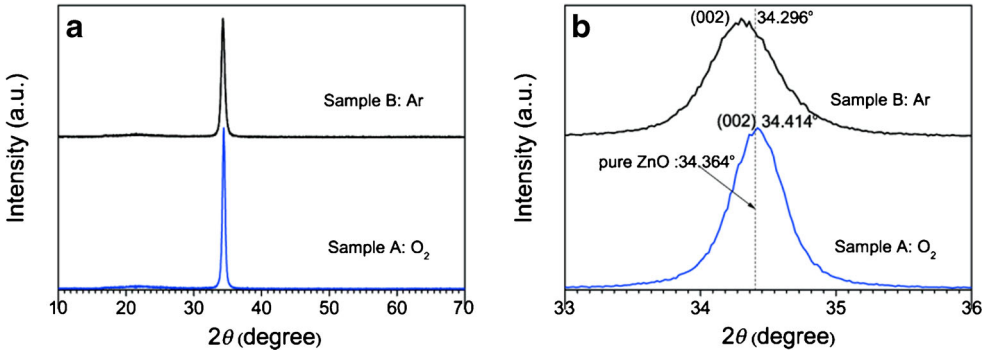

Figure 1. XRD patterns of Li-doped ZnO films annealed under O_2 and Ar ambient (**a**) and (002) diffraction peak position shifting as changing annealing ambient (**b**).

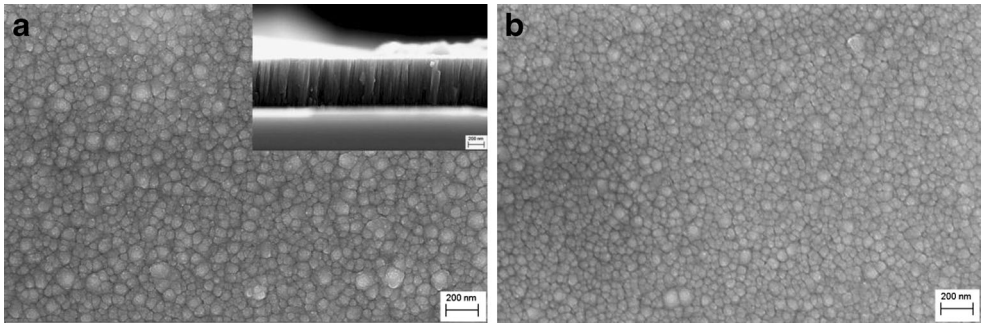

Figure 2. SEM micrographs of ZnO films annealed under O_2 ambient (**a**) and Ar ambient (**b**).

sample A are obviously thinner than of sample B, which indicate that sample A has better crystal structure.

Figure 1 (b) shows (002) diffraction peak position shifting as changing annealing ambient. Compared with pure ZnO, (002) diffraction peak position of both samples shifted because lithium ion is incorporated into ZnO crystal lattice to bring asymmetry of crystal lattice. According to Bragg formula, the crystal lattice expansion made diffraction peak shift to small angle, on the other hand, the crystal lattice shrink made diffraction peak shift to big angle. Because lithium ion radius is smaller than zinc ion radius lithium ion at substitution sites (Li_{Zn}) results in crystal lattice shrink and lithium ion at interstitials sites (Li_i) results in crystal lattice expansion. From figure 1(b), diffraction peak position of sample A shifted to big angle and that of sample B shifted to small angle, which proved lithium ion at substitution sites for sample A and at interstitials sites for sample B.

Figure 2 presents SEM micrographs of ZnO films annealed under O_2 (sample A) and Ar (sample B). Both films have uniform thickness and dense surface without visible pores. The average grain size of both films are approximately 70 ~ 90 nm along *c*-axis orientation. The inset in figure 2(a) is taken from the cross-section of sample A, which indicates that films have very dense columnar structure and the thickness is ~400 nm that agrees with the thickness measured by means of quartz vibration frequency.

3.2 *Electrical and optical properties*

Electrical properties of Li-doped ZnO films were examined by Hall effect measurement. Table 1 summarizes electrical properties of Li-doped ZnO thin film annealed under various ambients. The insulating quartz substrates used here can assure that the measured conduction property comes from ZnO films. It is obvious that the electrical properties of ZnO films are dependent on the annealing ambient. When annealing ambient is O_2, *p*-type conduction are observed and the resistivity is 78·61 Ω cm. However, when annealing ambient is Ar, the resistivity decreased greatly to 0·51 Ω cm and the conduction converted to *n*-type. The electrical properties of ZnO films had changed greatly because Li-related defects in ZnO occur at different sites (Iwata *et al* 2000; Nakagawa *et al* 2005; Qin *et al* 2009). As a result, ZnO film annealed under Ar ambient presents *n*-type conduction with low resistivity due to Li incorporation at interstitials sites (Lee *et al* 2006). On the other hand, ZnO film annealed under O_2 ambient showed *p*-type conduction due to Li incorporation at substitutional sites (Park *et al* 2002). Each zinc atom can provide two 4*s* electrons to O atom to fill up, 2*p* states while Li can only provide one single 2*s* electron. Hence, LiZn centre is an acceptor and *p* conduction is observed in ZnO. Meanwhile, Li can also lose its outermost electron acting as a donor and *n* conduction is observed in ZnO.

Table 1. Electrical properties of Li-doped ZnO films annealed at various ambients.

Sample	Annealing ambient	Conduction type	Resistivity (Ωcm)	Hall mobility (cm^2/vs)	Carrier concentration (cm^{-3})
A	Ar	n	0·51	5·08	$5{\cdot}61 \times 10^{18}$
B	O_2	p	78·61	1·02	$6{\cdot}48 \times 10^{16}$

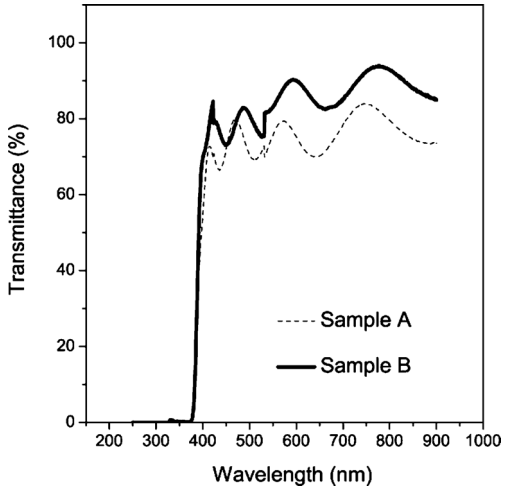

Figure 3. Transmittance spectra of ZnO:Li films treated under various annealing ambients.

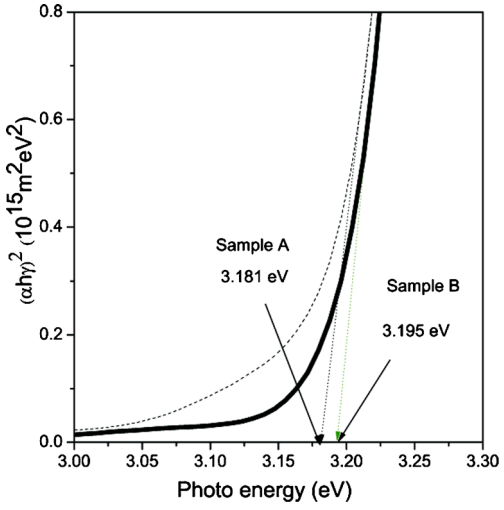

Figure 4. Plot of $(\alpha h\nu)^2$ vs $h\nu$.

Additionally, transmittance spectra of ZnO:Li films treated under various annealing ambients are shown in figure 3. Good transparency expands the insight into the application of ZnO films as transparent *p–n* joint. The average transmission of sample A annealed under O_2 ambient is ∼85% in visible spectral region, which is higher than that of sample B (∼80%). Because ZnO films annealed under O_2 ambient have perfect stoichiometric ratio and crystal structure, which agrees with XRD results.

In the direct transition semiconductor, optical bandgap of the films can be evaluated by plotting $(\alpha h\nu)^2$ vs $h\nu$, as shown in figure 4. The optical bandgap (E_g) can be calculated by the following equation:

$$(\alpha h\nu)^2 = C^2(h\nu - E_g), \tag{1}$$

$$\alpha = [2 \cdot 303 \times \log(1/T)]/d, \tag{2}$$

where α is the optical absorption coefficient, E_g the optical bandgap, C a constant and d the thickness of film. By this way, the optical bandgap (E_g) was estimated to be 3·181 eV for sample A and 3·195 eV for sample B, respectively. As a result, optical bandgap of sample B is different from that of sample A, which further indicated that Li incorporation may occur at different sites.

3.3 *Formation energies calculation*

Figure 5 shows ball and stick model of relaxed Li-doped wurtzite ZnO. When Li is substituted for Zn atom (Li_{Zn}), the lattice parameters a, c and c/a are 0·3167, 0·5094 and 0·1608 nm, respectively. When Li atoms reside at interstitial sites, we study the configurations of Li atom both at the octahedral ($Li_{i(O)}$) and tetrahedral ($Li_{i(T)}$) sites. In the case of Li interstitial at octahedral site, the lattice parameters a, c and c/a are 0·3193, 0·5146 and 0·1611 nm, respectively. When Li atoms are sited at tetrahedral interstitial site, the lattice parameters a, c and c/a are 0·3180, 0·5193 and 0·1633 nm, respectively.

Based on the above ball and stick model, formation energies of some single defects are calculated under various annealing ambients. The formation energies of these defects are obtained by total energy calculation as given below:

$$E_f = E(D) - E(0) + \Delta n_{Zn}\mu_{Zn} + \Delta n_O\mu_O + \Delta n_p\mu_p, \tag{3}$$

where $E(D)$ and $E(0)$ denote energies of the supercell with and without defect, respectively. $\triangle n$ is the number of ions (Zn, O or Li) charged between a perfect cell and its corresponding reservoir to form a defect. μ is the chemical potential of the corresponding reservoir. The upper limits for μ_{Zn} and μ_O are determined as the total energies of metallic Zn and gaseous O_2 per atom, respectively. As the net exchange rate of ions between ZnO and Zn and O reservoirs should be

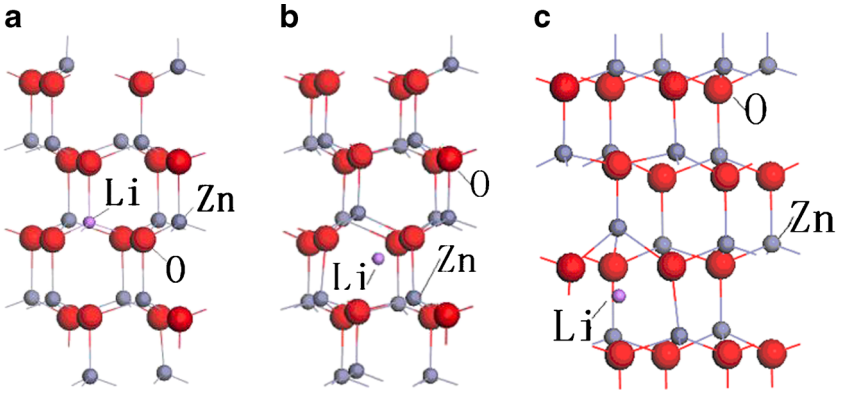

Figure 5. Ball and stick model of relaxed Li-doped wurtzite ZnO: (**a**) Li substitution at Zn (Li_{Zn}), (**b**) Li interstitial on octahedral site ($Li_{i(O)}$), (**c**) Li interstitial on tetrahedral site ($Li_{i(T)}$). Blue, red and purple balls represent Zn, O and Li ions, respectively.

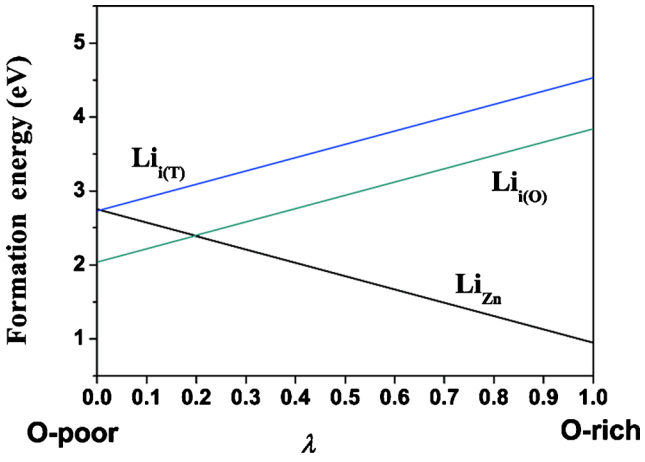

Figure 6. Formation energies of Li-related defects in O-poor and O-rich environments.

zero at equilibrium condition. μ_{Zn} and μ_O should also satisfy the relation $\mu_{Zn} + \mu_O = \mu_{ZnO}$. In order to describe μ_{Zn} and μ_O under various circumstances, we define a parameter (λ), which varies between 0 and 1 under extreme O-poor and O-rich conditions, respectively. We can formulate μ_{Zn} and μ_O as follows:

$$\mu_{Zn} = \mu_{Znmetal} - \lambda \Delta H, \tag{4}$$

$$\mu_O = \mu_{O2}/2 - (1 - \lambda)\Delta H, \tag{5}$$

where ΔH is the formulation heat of ZnO and its calculated value is 3·00 eV. The results are shown in figure 6.

Figure 6 shows formation energies of Li-related defects in O-poor and O-rich environments. Li in the octahedral cage ($Li_{i(o)}$) have the lowest energy among these Li-related defects under poor-O_2environment. It was supposed that $Li_{i(o)}$ were easier to exist than the others under poor O_2. As λ increases, the formation energy of both $Li_{i(o)}$ and $Li_{i(t)}$, defects increase and the formation energy of Li_{Zn} decreases. When λ reaches a certain value, the formation energy of Li_{Zn} was lower than that of $Li_{i(o)}$. Under O-rich side, Li_{Zn} has the lowest formation energies compared with other Li-related defects. It was supposed that Li_{Zn} was easy to exist under O-rich environment in view of the formation energies. In addition, the formation energy of $Li_{i(O)}$ was lower than that of $Li_{i(t)}$ under any environment. Therefore, Li at octahedral site is more stable than tetrahedral site, which are energetically preferable and located at octahedral interstitial. As a result, some amount of Li_{Zn} defect had existed in ZnO under O-rich environment and an amount of $Li_{i(o)}$ defect had existed in ZnO under O-poor environment, which was in good agreement with the above experimental value.

4. Conclusions

In summary, Li-doped ZnO thin films were grown on quartz substrates by radio frequency magnetron sputtering and *in situ* annealing under O_2 ambient or Ar ambient. Li-related defects in ZnO films strongly depend on the annealing ambient oxygen pressure. Both ZnO films treated under O_2 ambient or Ar ambient possessed a good crystallinity with *c*-axis orientation, uniform thickness and dense surface. Electrical and optical properties demonstrated that Li_{Zn} defects existed in ZnO films under O_2-rich ambient and Li_i defects existed in ZnO films under O_2-poor ambient, which were testified by calculating formation energies of Li-doped ZnO.

Acknowledgements

This work was supported by the Research Foundation of Education Bureau of Liaoning Province, China (No. L2011098), the Foundation for Key Program of Ministry of Education, China (No. 212031) and the National Nature Science Foundation of China (No. 51074087).

References

Coppa B J, Davis R F and Nemanich R J 2003 *Appl. Phys. Lett.* **82** 400

Hu J, He H Y and Pan B C 2008 *J. Appl. Phys* **103** 113706

Iwata K, Fons P, Yamada A, Matsubara K and Niki S 2000 *J. Cryst. Growth* **209** 526

Joseph M, Tabata H, Saeki H, Ueda K and Kawai T 2001 *Physica B* **302/303** 140

Lee W J, Kang J and Chang K J 2006 *Phys. Rev. B* **73** 024117

Look D C and Claflin B 2004 *Phys. Status Solidi B* **241** 624

Look D C, Claflin B, Alivov Y I and Park S 2004 *Phys. Status Solidi A* **201** 2203

Look D C, Reynolds D C, Litton C W, Jones R L, Eason D B and Cantwell G 2002 *Appl. Phys. Lett.* **81** 1830

Mohamed G A, Abd El-Moiz A B and Rashad M 2005 *Physica B* **370** 158

Nakagawa T, Sakaguchi I, Matsunaga K, Yamamoto T, Haneda H and Ikuhara Y 2005 *Meth. Phys. Res. B* **232** 343

Osamu N, Toru S, Takahiro M, Seiichi A, Hitoshi T and Tomoji K 2000 *Appl. Phys. Lett.* **77** 3257

Park C H, Zhang S B and Wei S H 2002 *Phys. Rev. B* **66** 073202

Qin R *et al* 2009 *Phys. Chem. C* **113** 9541

Shan F K, Liu G X, Lee W J and Shin B C 2007 *J. Appl. Phys.* **101** 053106

Van de Walle C G 2000 *Phys. Rev. Lett.* **85** 1012

Zhang S B, Wei S H and Zunger A F 2001 *Phys. Rev. B* **63** 075205